JET–P(98)04

Theory of Alfvén Eigenmode Instabilities and Related Alpha Particle Transport in JET D-T Plasmas

W Kerner, D Borba[1], S ESharapov, B N Breizman[2], J Candy[2], A Fasoli[3], L C Appel[4], R Heeter[5], L-G Eriksson, M Mantsinen[6].

JET Joint Undertaking, Abingdon, Oxfordshire, OX14 3EA,
[1] Associaçáo EURATOM/IST Av Rovisco Pais 1096 Lisbon, Portugal.
[2] Institute for Fusion Studies, The University of Texas at Austin, Texas, USA.
[3] CRPP-EPFL, Ass. Euratom-Swiss Confederation, CH-1015, Lausanne, Switzerland.
[4] UKAEA Fusion, Culham, Abingdon, Oxfordshire, OX14 3DB, UK.
[5] Princeton Plasma Physics Laboratory, P.O. Box 451, Princeton, NJ 08543, USA.
[6] Helsinki University of Technology, Association Euratom-Tekes, Espoo, Finland.

Preprint of a Paper to be submitted for publication in Nuclear Fusion

February 1998

ABSTRACT.

Linear and nonlinear models for anomalous alpha particle transport due to collective instabilities are reviewed. The linear stability analysis is applied to the comparison of measured and computed Alfvén Eigenmodes in tokamaks ("spectroscopy"). Scenarios for nonlinear wave evolution and fast ion redistribution are discussed.

1. INTRODUCTION

Early in the development of plasma theory it was realised that super-thermal particles can drive plasma waves unstable through resonant particle-wave interaction [1,2]. In D-T plasmas the fusion born alpha particles with energies around 3.5 MeV have initially super-Alfvénic velocity and will in the slowing-down process eventually match the Alfvén velocity $v_A = B/(4\pi\rho)^{1/2}$, where B denotes the magnetic field and ρ the mass density (e.g. $\rho = n_i m_i$). This implies that the resonant interaction of alpha particles with Alfvén waves is an important issue. The confinement of alpha particles in tokamaks is being studied extensively in actual experiments as well as conceptually in the design of the fusion test reactor ITER. It is crucial for a reactor that the alpha particle transport is either classical or moderately anomalous and therefore tolerable. So far all tritium discharges performed at TFTR and at JET support the claim that the alpha particles are sufficiently well confined.

The great uncertainty with respect to the extrapolation towards the break-even condition at JET or, even further, towards an ignited tokamak plasma is the anomalous alpha particle transport due to collective instabilities caused by the free energy in the alpha particles (or in the energetic ions in general). For sufficiently large amplitude of the perturbed field anomalous transport of energetic ions can occur. Such losses have been observed in DIII-D experiments at low field with NBI power, where the injected ions match the Alfvén velocity. As shown in Fig. 2 of Ref. [3], a large number of beam ions are expelled, (seen as a drop in the neutron emission) during bursts of TAE observed on a magnetic pick-up coil. Similar degradation of the alpha particle confinement in a reactor would reduce the ignition margin and cause serious damage to the first wall. The physics issues related to the effect of Alfvén waves on the alpha confinement can be addressed in various ways, which do not always require tritium discharges.

First, the spectrum of Alfvén waves can be analysed and the existence of weakly-damped Alfvén Eigenmodes (AE) checked. This can be done by antenna excitation without the involvement of energetic ions. At JET such external excitation of AE's has been studied with the use of the Saddle Coils [4-6]. The low-n wave number spectrum of AE's has been measured and analysed in detail. These studies have confirmed the existence of weakly damped AE localised in the plasma centre.

Second, the excitation of such AE by NBI and RF generated fast ions can be studied. In present tokamaks up to 30 MW of heating through NBI is provided. Then, with beam energies in

the range of 100-160 keV the Alfvén resonance is reached only for low magnetic field of 1T. The RF heating can generate energetic ions with tail energies in excess of 0.5 MeV, which can resonate with the AE. ITER will rely on 50 to 100 MW of additional heating power for reaching ignition. Since the injected ions will have much higher energies than used presently, resonant interaction with beam ions as well as RF tail ions needs to be studied in addition to the alpha-particle interaction. Present tokamak experiments which demonstrate losses of energetic ions due to collective instabilities yield a great deal of information suitable for benchmark tests of the large-scale codes.

Finally, the alpha particle confinement can be studied in tritium discharges. The detailed analysis should confirm the validity of the theoretical models and the key physics ideas - or should indicate new development - which is essential for accurate predictions in performance of tokamak-reactor plasmas.

In this paper we analyse linear stability and nonlinear evolution of Alfvén waves by comparing measured spectra with theoretical models. The numerical tools for such an analysis are described. The plan of the paper is as follows:

In Section 2 the hybrid fluid-particle model is presented which takes into account the power transfer between particles and waves in the linear phase. The numerical evolution is performed by means of the CASTOR-K code package. The Alfvén spectrum as observed on JET discharges is discussed in detail. Section 3 is devoted to the weak turbulence model which describes the nonlinear evolution of the system. The algorithms employed by the codes FAC and HAGIS are outlined. The different classes of nonlinear scenarios are discussed and compared with experimental observations. Finally, in Sec. 4, conclusions are presented.

2. HYBRID FLUID - PARTICLE MODEL

In our simulations of collective modes in fusion plasmas, we describe the “bulk” ions and electrons by macroscopic MHD equations. These yield an appropriate model for equilibrium and stability, as well as for plasma oscillations such as Alfvén waves. Fusion born alpha particles have super-thermal energies of about 3.5 MeV and are well described by a slowing down distribution. Their pressure is a finite fraction of the bulk plasma pressure (typically 10% to 20%). Neutral beam injection and resonant radio frequency heating may also generate super-thermal ions with pressure comparable to the bulk ion pressure. The influence of these fast ions on the bulk plasma is incorporated in the equilibrium profiles which are reconstructed from measurements. The power transfer from the energetic ions to plasma waves is taken into account in the δW_{hot} functional, which yields the growth rate and the damping of the MHD wave in the linear phase. This particle-wave interaction may also lead to a branch of plasma instabilities known as energetic particle driven modes, or EPM. Only particles which are close to resonant regions in phase space can exchange a considerable amount of energy with the MHD wave, and these particles get trapped inside the potential well created by the MHD perturbation. Eventually the

drive is reduced nonlinearly by a relaxation of the energetic particle distribution function and is accompanied by saturation of the wave amplitude. This nonlinear process is computed using a particle simulation model for the fast ions which will be described in Sec.3. These numerical models have been developed for general tokamak configurations. The family of codes used at JET is described in Fig. 2.1. Starting from the discharge equilibrium profiles, the spectrum of ideal and resistive (kinetic) MHD normal modes is computed by the MHD codes MISHKA-1 (ideal, incompressible) [7] and CASTOR (resistive, compressible) [8]. The linearised MHD solution for the plasma normal modes and the gyrokinetic perturbative contribution for the energetic particles can be combined into a dispersion relation of the form

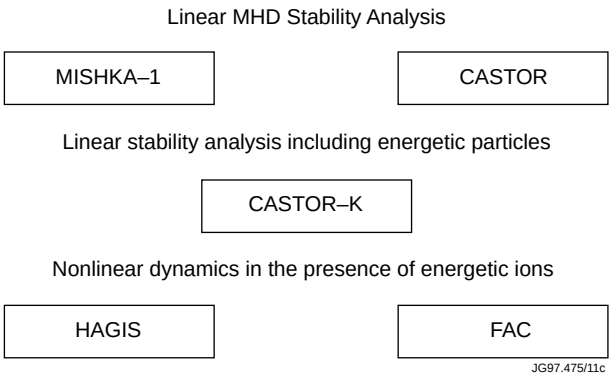

Fig. 2.1 Family of fluid-particle codes used at JET.

$$\omega^2 E_k = W_{mhd} + \delta W_{hot}(\omega) \,, \tag{2.1}$$

where the power transfer is quantified by the quadratic form $\delta W_{hot}(\omega)$ and is evaluated by the kinetic extension of the CASTOR code called CASTOR-K. The nonlinear evolution of these normal modes is subsequently computed using the δf particle codes FAC and HAGIS — developed at JET in collaboration with IFS Texas and UKAEA. We give now a short description of the three different levels of the plasma description.

2.1 Normal Mode Description

The plasma equilibrium obeys force balance

$$-\nabla P + \mathbf{J} \times \mathbf{B} = 0 \,, \tag{2.2}$$

where P is the pressure, **J** the current, and **B** the magnetic field. For numerical solution, Eq. (2.2) is cast into the Grad-Shafranov form. The normal-mode analysis considers small perturbations around the equilibrium state and is performed by means of the linear spectral codes CASTOR and MISHKA [7, 8]. The time behaviour is expressed by an eigenvalue λ in the form

$$\zeta(\mathbf{r}, t) = e^{\lambda t}\, \zeta(\mathbf{r}) \,. \tag{2.3}$$

The imaginary part of λ describes oscillatory behaviour with frequency $\omega = \mathrm{Im}\,(\lambda)$, whereas the real part $\gamma = \mathrm{Re}\,(\lambda)$ corresponds to exponentially growing ($\gamma > 0$) or damped ($\gamma < 0$) motion. The linear eigenfunctions computed by CASTOR and MISHKA and reported in this paper, are solutions of the linearised, compressible MHD equations in dimensionless form:

Continuity:

$$\lambda\delta\rho = -\nabla\cdot\left(\rho_0\delta\dot{\nu}\right) \tag{2.4}$$

Momentum:

$$\lambda\rho_0\ \delta\dot{\nu} = -\nabla\cdot\left(\rho_0\delta T + \delta\rho T_0\right)$$

$$+\left(\nabla\times\dot{B}_0\right)\times\left(\nabla\times\delta\dot{A}\right) - \dot{B}_0\times\left(\nabla\times\nabla\times\delta\dot{A}\right)$$

Energy:

$$\lambda\rho_0\ \delta T = -\rho_0\delta\dot{\nu}\cdot\nabla T_0 - (\Gamma-1)\rho_0\nabla\cdot\delta\dot{\nu}$$

$$+ 2\eta(\gamma-1)\left(\nabla\times\dot{B}_0\right)\cdot\left(\nabla\times\nabla\times\Gamma\dot{A}\right)$$

Faraday's Law:

$$\lambda\delta\dot{A} = -\dot{B}_0\times\delta\dot{\nu} - \eta\nabla\times\nabla\times\delta\dot{A}$$

Here $\delta\rho$ denotes the density, $\delta\mathbf{v}$ the velocity, δT the temperature and $\delta\mathbf{A}$ the vector potential such that $\delta\mathbf{B} = \nabla\times\delta\mathbf{A}$. Also, η is the resistivity and Γ the ratio of specific heats. This formulation includes both density and temperature instead of pressure.

The inclusion of resistivity in Eqs. (2.4) makes the computation of all unstable resistive eigenmodes feasible. However, in the context of the Alfvén eigenmode physics the resistive terms are only used to resolve the singularities of eigenmodes crossing the Alfvén continua. These singularities are resolved by matching the outer ideal solution to the layer physics, which includes kinetic effects in terms of Finite Larmor Radius (FLR) ρ_i and non-vanishing parallel electric field [9-12]. It has been demonstrated that these nonideal effects can be taken into account in the CASTOR model by a "complex resistivity" [13] in Ohm's law:

$$\delta\dot{E} + \delta\dot{\nu}\times\dot{B} = \eta_{\|}\,\delta\dot{J}_{\|}\,, \tag{2.5}$$

with

$$\eta_{\|} \sim i\omega\,\rho_i^2\left(1 - i\delta_e\right) \tag{2.6}$$

where δ_e arises from collisional friction between trapped electrons and passing particles and is computed from the bounce-averaged electron kinetic equation.

2.2 Spectrum of Alfvén Waves in Tokamaks

The spectrum of Alfvén waves can be studied experimentally by antenna excitation, i.e. without the existence of super-thermal ions. This enables an active probing of the type and structure of

Alfvén Eigenmodes (AE) and their damping. On JET the Saddle Coils have been used as an exciter where the frequency can be scanned between 20 and 500 kHz. By synchronous detection the plasma response to the antenna can be measured very accurately and the damping can be quantified. It has been successfully demonstrated that with an antenna power of less than 10 kW plasma normal modes in the range of the Alfvén frequency AE can be excited [4-6]. When the applied frequency matches the frequency of a plasma normal mode there occurs a sharp peak in the absorption spectrum, and the width of this peak is proportional to the damping of this specific normal mode.

A typical result as modelled by the CASTOR code for this antenna excitation is displayed in Fig. 2.2, where the coupled power is computed as a function of the antenna frequency. Regions of broad spectral response indicate the presence of plasma continuum damping. In these regions, every magnetic field line oscillates with its own local Alfvén frequency, thereby giving rise to a continuum of normal modes in radius. When a wave is launched into such a region, this wave experience a “friction” due to the very different local propagation of the continuum modes. Consequently, the resulting continuum damping is proportional to the gradients in the equilibrium profiles. Since the continuum modes are localised on a specific flux surface, a simplified version of the CASTOR code needs to be solved only on every flux surface separately. The corresponding CSCAS code [14], makes feasible the efficient and fast evaluation of the continuum structures of many equilibria. If such a damping would occur uniformly in the plasma volume it would be very difficult to excite and destabilise AE by both antenna and fast ion drive. However, there exist pronounced gaps in the Alfvén continua due to coupling caused by finite toroidicity (toroidal gap), elongation (elliptical gap) and other effects which break the cylindrical symmetry. This coupling leads to “forbidden crossings” of continuum modes, i.e. gaps. Furthermore, new global Alfvén eigenmodes exist in these gaps with zero or, in the case of several gaps at different radial positions, small damping. In Fig. 2.2 the toroidal gap around w.(R/v_A) ~ 0.5 and the elongation induced gap around w . (R/v_A) ~ 1.3 are clearly seen. In addition, toroidicity induced AE (TAE) and elongation induced AE (EAE) exist with very small damping. For high beta an additional AE occurs at lower frequency, the so-called beta induced AE (BAE). If the plasma is sufficiently hot kinetic effects, which are characterised by the kinetic coupling factor [9-13]

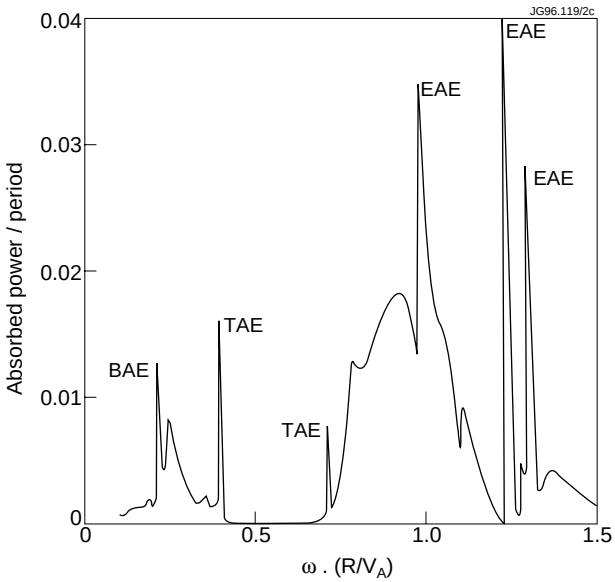

Fig. 2.2 The plasma response as a function of the antenna frequency computed by CASTOR.

$$\lambda_k = 4\rho_i \frac{m}{r_g} \frac{S}{\varepsilon^{3/2}} \sqrt{\frac{3}{4} + \frac{T_e}{T_i}} , \qquad (2.7)$$

where ρ_i denotes the Larmor radius, m the dominant poloidal Fourier harmonic, r_g the radius of the gap, S the magnetic shear and $\varepsilon = 3.5\ r_g/R$ the local inverse aspect ratio, need to be considered. This coupling causes the continuum to break up into the kinetic Alfvén spectrum which can be obtained from the linear resistive spectral codes CASTOR and MISHKA by matching the complex resistivity (2.6) with the non-ideal parameter λ_k (2.7). On the bottom of the toroidal gap this coupling causes a large amount of energy to be carried away radially, which is eventually absorbed in the cold plasma edge. The resulting damping, the radiative damping, is quite large. This damping of the TAE's whose eigenfrequencies are on the bottom of the TAE-gap is clearly seen on Fig.2.3. in form of a broad absorbtion. On the top of the gap a new class of kinetic TAE, called KTAE, exists which are characterised by small damping and roughly equal spacing in frequency

$$\omega = \omega_o + p\,\Delta\omega \text{ for } p = 0, 1, 2, ... \qquad (2.8)$$

It is noted that the different poloidal Fourier harmonics m and m + 1 of the TAE have equal parity which results in a ballooning - like, poloidal mode structure, whereas the KTAE have opposite parity resulting in an anti-ballooning structure. The lowest KTAE for small magnetic shear values degenerates into the core-localised low-shear TAE and can be usually found already in ideal MHD - as is evident from Fig. 2.2. The fine-splitting due to kinetic effects has been clearly identified in the antenna excitation experiments [5]. Similar splitting is found for RF driven AE on the top of the elongation induced gaps as will be discussed in more detail later.

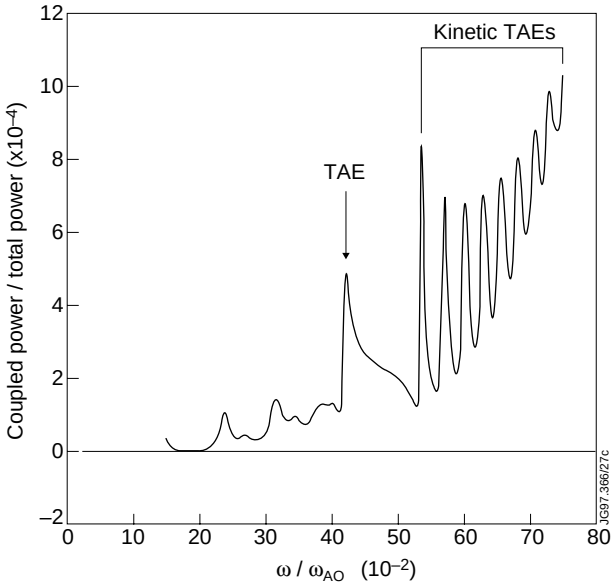

Fig. 2.3 Kinetic effects on AE's: The plasma response as a function of the antenna frequency computed by CASTOR using complex resistivity.

2.3 Energetic Particle Driven Instabilities

The AE excitation experiments – based on antenna drive as well as on NBI and RF generated fast ions – have confirmed that in the case of weak drive only MHD normal modes are excited. Weak drive does not imply low heating power; rather, it refers to a small power density. The free energy for the destablisation is actually caused by the gradient of the fast particle pressure. Thus

the perturbative method can be applied, where the frequency ω and the eigenfunction ξ (**r**) are determined by MHD and can be obtained by the MISHKA-1 or CASTOR code.

The power transfer between the wave and the particle is given by the six dimensional phase-space integral

$$\delta W_{hot} = -\frac{1}{2}\int d^3x\, d^3v\, L^{(1)^*} f_1. \tag{2.9}$$

where $L^{(1)}$ is the perturbed Lagrangian of the wave-particle interaction and f_1 the perturbed distribution function, which is obtained by integrating the linearised Vlasov equation along the particle trajectories for a given fast particle distribution F_o. The growth rate or damping factor is extracted from the imaginary part of δW_{hot}

$$\gamma = \frac{\omega_i}{\omega_r} = \frac{\mathrm{Im}\left[\delta W_{hot}\right]}{2\omega_r^2 E_k}\ . \tag{2.10}$$

Since only the non-adiabatic part of f_1 can give an imaginary contribution to the dispersion function, it is only necessary to consider

$$\delta W_{hot} = -\frac{1}{2}\int d^3x d^3v \left(\omega\frac{\partial F_0}{\partial E} - n_o\frac{\partial F_0}{\partial P_\phi}\right) L^{(1)} * \int_{-\infty}^{t} L^{(1)} d\tau. \tag{2.11}$$

with additional integration over the time.

For Alfvén waves or marginally stable MHD modes the perturbed Lagrangian reduces to

$$L^{(1)} = -\left(mv_\parallel^2 - \mu B\right)\boldsymbol{\xi}\cdot\boldsymbol{\kappa} + \mu B\nabla\cdot\boldsymbol{\xi}_\perp\ , \tag{2.12}$$

where κ denotes the curvature of the equilibrium magnetic field and μ is the magnetic moment. It is convenient to introduce new phase-space variables through the transformation (**x, v**) → (P_ϕ, ϕ, E, τ, μ, α), where τ is the time along the orbit. The Jacobian of this transformation is a constant:

$$d^3x d^3v = \left(\frac{c}{Zem^2}\right)\sum_{\sigma=\pm} dP_\phi dE\ d\mu\ d\tau\ d\phi\ d\alpha \tag{2.13}$$

P_ϕ denotes the toroidal canonical momentum, E the energy, α the gyrophase and ϕ the toroidal angle. Carrying out the integration over τ, ϕ and α, δW_{hot} reduces to [15]

$$\delta W_{hot} = -\frac{2\pi^2}{Zem^2}\sum_\sigma \int dP_\phi dE d\mu \sum_{\tilde{\rho}=-\infty}^{\infty} \tau_b\left(\omega - n_o\omega_*\right)\frac{\partial F}{\partial E}\frac{|Y_{\tilde{\rho}}|^2}{\omega + n_o\omega_D + \left(n_o q + \tilde{\rho}\right)\omega_b}\ , \tag{2.14}$$

where ω_b and τ_b are the bounce frequency and bounce time, and ω_D the toroidal precession frequency. The perturbed Lagrangian is bounce averaged over the particle orbits and expanded in Fourier harmonics of the periodic particle motion

$$L^{(1)} = \hat{L}^{(1)} e^{-in_o\phi(\tau)} , \tag{21.15}$$

with n_o the toroidal wave number. The Fourier coefficients are defined as

$$Y_{\tilde{\rho}} = \oint \frac{d\tau}{\tau_b} \tilde{L}^{(1)} e^{i\tilde{\rho}\omega_b\tau} \tag{2.16}$$

This procedure allows one to decompose the periodic motion in the f-direction for both passing and trapped particles. The denominator in the dW_{hot} expression vanishes if

$$\Gamma\left(E, P_\phi, \mu\right) = \omega + n_o\omega_D + \left(n_o q + \tilde{\rho}\right)\omega_b = 0 , \tag{2.17}$$

which is the wave-particle resonance condition. The singularities of the integrand have to be taken into account in the integration over phase space. The term proportional to ω represents the free energy due to the gradients in velocity space, giving rise to Landau damping, while the term proportional to $n_o\omega_*$ represents the free energy due to spatial gradients in the distribution function

$$\omega_* = \frac{\partial F}{\partial P_\phi} \Big/ \frac{\partial F}{\partial E} \tag{2.18}$$

The drive is proportional to the toroidal wave number n_o through the combination $n_o\,\omega_*$ in Eq. (2.17). However with increasing toroidal mode number the radial width of the eigenfunction decreases and the mode width becomes equal to the orbit width, so that the particle-to-wave power transfer saturates. This indicates that the fast ion orbits have to be treated in full generality. This saturation in the destabilisation sets in for JET plasmas for toroidal mode numbers between ten and fifteen, $n_o \sim 10\text{-}15$. In the evaluation of the growth rate it is only necessary to compute the imaginary part of δW_{hot}. Since only the poles in the particle wave response can give an imaginary contribution to δW_{hot}, the three dimensional integral is reduced to two dimensions by an integration subject to the resonance condition $\Gamma(E, P_\phi, \mu) = 0$ In the evaluation of the growth rate the δW_{hot} quadratic form is reduced to

$$\delta W_{hot} = -\frac{2\pi^2}{\Omega m^2} \int dP_\phi d\mu \sum_{\sigma=\pm} \sum_{\tilde{\rho}=-\infty}^{\infty} \tau_b\left(\omega - n_o\omega_*\right) \frac{\partial F}{\partial E} \frac{2\pi i |Y_{\tilde{\rho}}|^2}{\frac{\partial \Gamma}{\partial E}} \tag{2.19}$$

The CASTOR-K code [16] evaluates the dW_{hot} functional for given plasma equilibrium, MHD eigenfunction and fast particle distribution F_o. This calculation has to be performed in the straight field line coordinate system $s = \sqrt{\psi / \psi_s}, \theta, \phi$, where the equilibrium magnetic field is represented by

$$\mathbf{B} = \nabla\phi \times \nabla\psi + F\nabla\phi \tag{2.20}$$

together with the corresponding metric g_{ik}, being characterised by the Jacobian

$$J_{CASTOR} = 2s\psi_S \frac{qR^2}{F} . \tag{2.21}$$

The scheme of the integration is summarised in Table I.

The gyro angle	α	analytical	average procedure
The poloidal angle	θ	numerical	Fourier transform
The toroidal angle	ϕ	analytical	Fourier decomposition
The energy	E	analytical	integration over the poles
The magnetic moment	μ	numerical	binary search algorithm
The toroidal canonical momentum	ρ_ϕ	numerical	binary search algorithm

The evaluation of δW_{not} requires the integration of fast particle orbits in the equilibrium fields. The trajectory of a particle can be expressed analytically as a function of the invariants of motion and of the equilibrium quantities. This method is used for orbit classification. This is essential for tracking all particle resonances. However, the time dependence of the particle coordinates must be integrated numerically. In order to improve the integrator accuracy, the coordinate system is changed into a poloidally Cartesian system when a particle gets close to the magnetic axis.

$$\begin{aligned} x &= s\cos\theta \\ y &= s\sin\theta \end{aligned} \tag{2.22}$$

An explicit integration procedure in terms of a fourth-order Runge-Kutta algorithm is used.

The remaining integration over the μ, P_ϕ co-ordinates is performed using a bi-dimensional adaptive scheme. The procedure works in two phases. At first a rectangular mesh is constructed evaluating the function to be integrated at each point. Thus, a first estimate of the integral is obtained. Secondly, a refinement criterion selects the area where accumulation points are required for improvement in the accuracy of the integration. This procedure is repeated until a predefined accuracy of the integration is achieved. The mesh accumulation is concentrated in

areas where the function is less well behaved and, hence, the contribution to the overall integration is more important. The method is a two-dimensional equivalent of Simpson's rule [17], where the evaluated points are fitted using cubic polynomials.

The accuracy of the CASTOR-K code has been tested by comparison with analytic results in the large aspect ratio and small orbit width limit and by benchmark tests with the NOVA-K code. This comparison has been satisfactory. The comparison with numerical results obtained by the non-linear codes FAC and HAGIS is displayed in Fig. 2.4. Over a wide range of parameters the agreement is good both in the small and large orbit width versions of the CASTOR-K code.

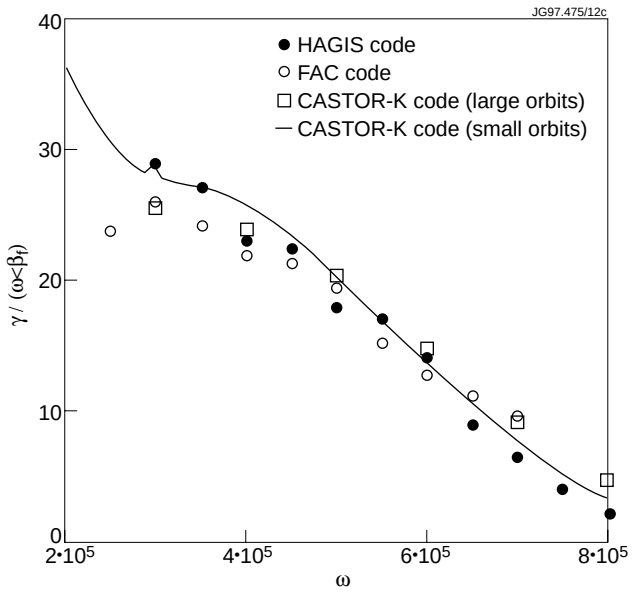

Fig. 2.4 Benchmark test on comparison of the dependence of the growth rate on the frequency.

2.4. Analysis of Experimental Observations on Jet

The results of the JET antenna excitation experiments have been described in Refs. [4-6]. Here we analyse AE activity observed in JET discharges with additional heating. It is emphasised that the NBI generated ions have energies around 150 KeV — which for 3T, 3MA discharges is well below the Alfvén resonance. In order to satisfy the Alfvén resonance condition $v_{beam} = v_A$, the field has to be smaller than 1T. Such plasmas are of no relevance for the DTE1 campaign. It is however possible to match the $v_A/3$ resonance in JET high performance plasmas. CASTOR-K calculations show that a destabilisation of AE can only occur for quite high toroidal mode numbers. For example the simulation of specific discharges has shown that AE's with n=14 become marginally unstable. There is no clear experimental identification of corresponding AE's.

This leaves us with the analysis of AE's driven unstable by the RF generated fast ions and by α-particles. There is clear experimental evidence that AE's are routinely observed when the heating power exceeds 4-5 MW, depending on the plasma density. In discharge #40328 the RF heating power is slowly ramped up from 3MW to 7MW. When P_{RF} exceeds 5MW a set of AE is observed, as is shown in Fig. 2.5, with toroidal mode numbers in the range $5 \le n \le 11$. The AE with larger mode numbers are excited first. This is consistent with the drive being proportional to $n\omega_*$ in Eq. (2.19). The drive levels off for $n \ge 10$, when the mode width becomes proportional to the orbit width. The instability drive is evaluated by the CASTOR-K code for increasing tail ion temperature in a Stix-type distribution,

$$F_0 \propto e^{-E/T} \times e^{-\left(\frac{\Lambda-\Lambda_0}{\Delta\Lambda}\right)^2};\ \Lambda_0 \sim 1; \Delta\Lambda \sim 0.01, \tag{2.23}$$

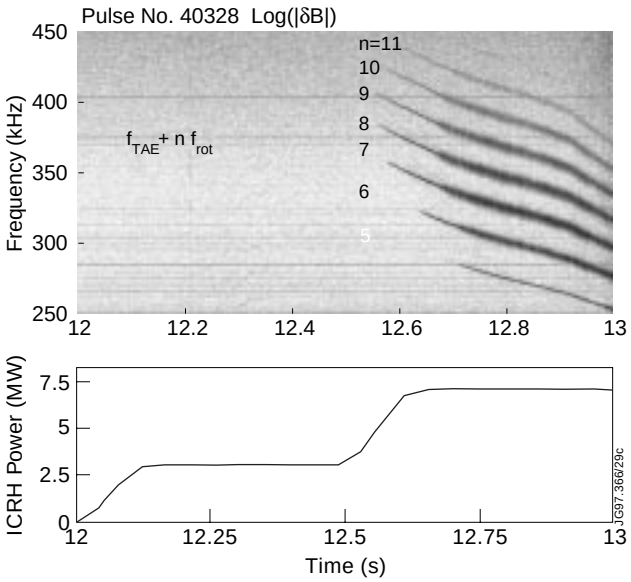

Fig. 2.5 Threshold for ICRH driven AE's.

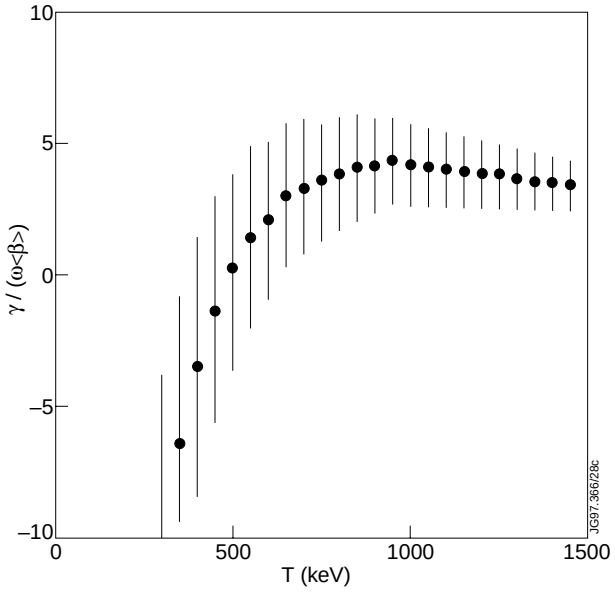

Fig. 2.6 Modelling of the growth rate of a n = 5 TAE in the presence of RF generated ions due to on-axis heating for a distribution $F \propto e^{-\frac{E}{T}} \times e^{-\left(\frac{\Lambda-\Lambda_0}{\Delta\Lambda}\right)^2}$ *($\Lambda_0 \sim 1$, $\Delta\Lambda \sim 0,01$ pitch angle).*

(where Λ denotes the pitch angle), which represents trapped particles with a banana tip close to the ICRH resonance layer. The resulting growth rate in dependence of the tail temperature is displayed in Fig. 2.6. The growth rate is normalised to the TAE frequency and to the averaged fast particle beta, as usual, since the drive is proportional to $<\beta_f>$. The calculation is complicated since particles with large and non-standard orbits are in resonance with the wave. The corresponding hatched region indicates the sensitivity of the result on details of the equilibrium profiles. In the case of the considered TAE with n = 5 the instability sets in for T_{tail} > (500-600) KeV. The reconstruction of the RF power deposition by the PION [18] and FIDO [19] codes shows that the energetic tail ions have an energy corresponding to 700 keV when $P_{RF} \approx 5$MeV. This agrees with the experimentally observed threshold. An independent assessment of the threshold by measuring the damping of low-n TAE for increasing RF power yields also a critical power of about 5MW [20]. The spectrogram of the frequency versus time reveals a sequence of frequencies, due to the Doppler shift

$$f = f_{TAE} + n\, f_{rot} \tag{2.24}$$

observed in the laboratory frame. In Fig. 2.7 this Doppler shift is subtracted. It is evident that the frequencies of AE with $4 \le n \le 9$ nearly coincide. The solid line underneath is a prediction of the

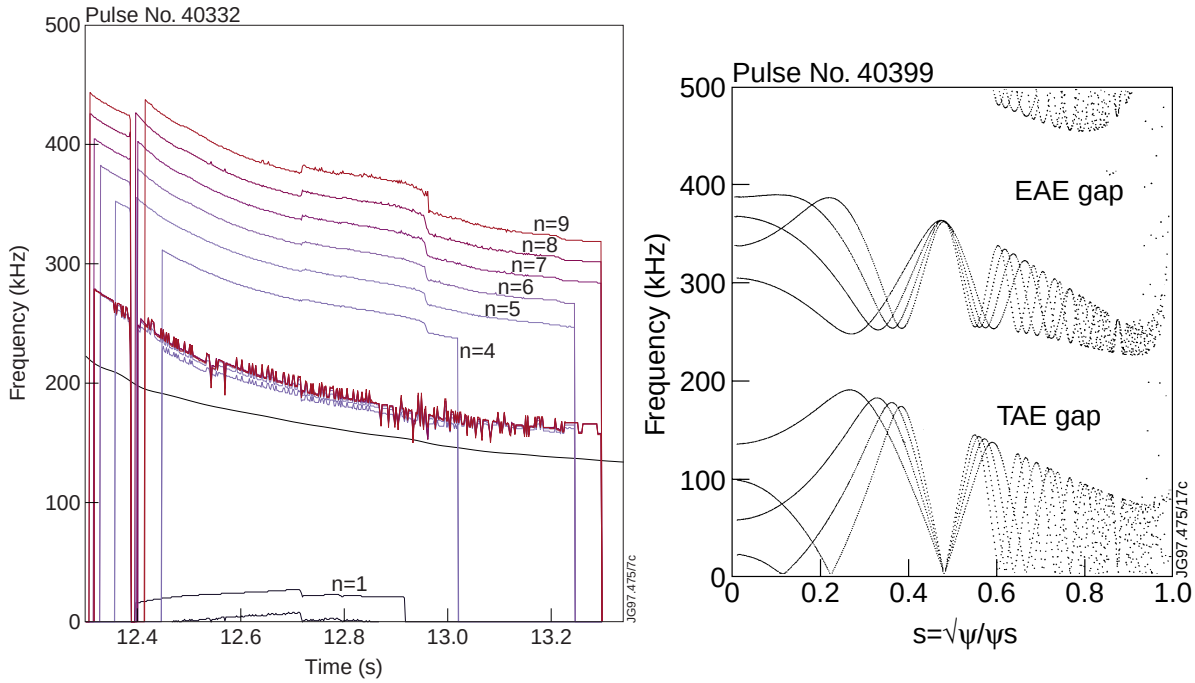

Fig. 2.7 AE activity on hot-ion H-mode discharge #40332: a) Spectrum: frequency versus time (The solid line indicates the prognosticated Alfvén frequency for central gap value for safety factors). b) Continuous spectrum gap structure.

TAE frequency for the actual electron density and the q value in the centre of the TAE gap. The density increases with the beam fuelling whereas the safety factor profile is almost constant in time. The agreement of the observed frequency with the theoretical frequency confirms the Alfvénic scaling of the wave. The Alfvén continuum structure is displayed on the second diagram on Fig. 2.7. At 52.8 s the observed frequency is $f_{TAE} \simeq 200\,\text{kHz}$ and corresponds to a location at the bottom of the TAE gap around s = 0.3 - 0.4 (note that s ≈ r/a). This corresponds to the location of the highest pressure gradient of the RF generated fast ion population. Toroidicity leads to a strong coupling between the m and m + 1 poloidal harmonics, which are characterised by even or odd parity with respect to the radial dependence. This leads to a pronounced ballooning - type (even parity) or anti-ballooning-type (odd parity) eigenfunction. From Fig. 2.8 it is seen that the ballooning structure of the TAE eigenfunction agrees well with the on - axis deposition of the RF power generating trapped ions on the low field side. Therefore, the observed magnetic signal is identified to be a TAE. The corresponding KTAE's with somewhat higher frequency and anti-ballooning eigenmode structure do not fit the observations well. These facts also make implausible the explanation of the observed fine-splitting of this TAE frequency into typically five sub-modes with $\Delta\omega \approx 1\text{kHz}$ by means of kinetic effects involving KTAE. An explanation in terms of non-linear effects has been proposed in Sec.4.

Next we analyse the observed AE activity in optimised shear discharges, where the safety factor is well above unity, i.e. $q_{min} \approx 1.7$. The spectrogram of discharge #40399, Fig. 2.9, shows in addition to the discussed TAE several modes in the elongation induced gap. Both classes of

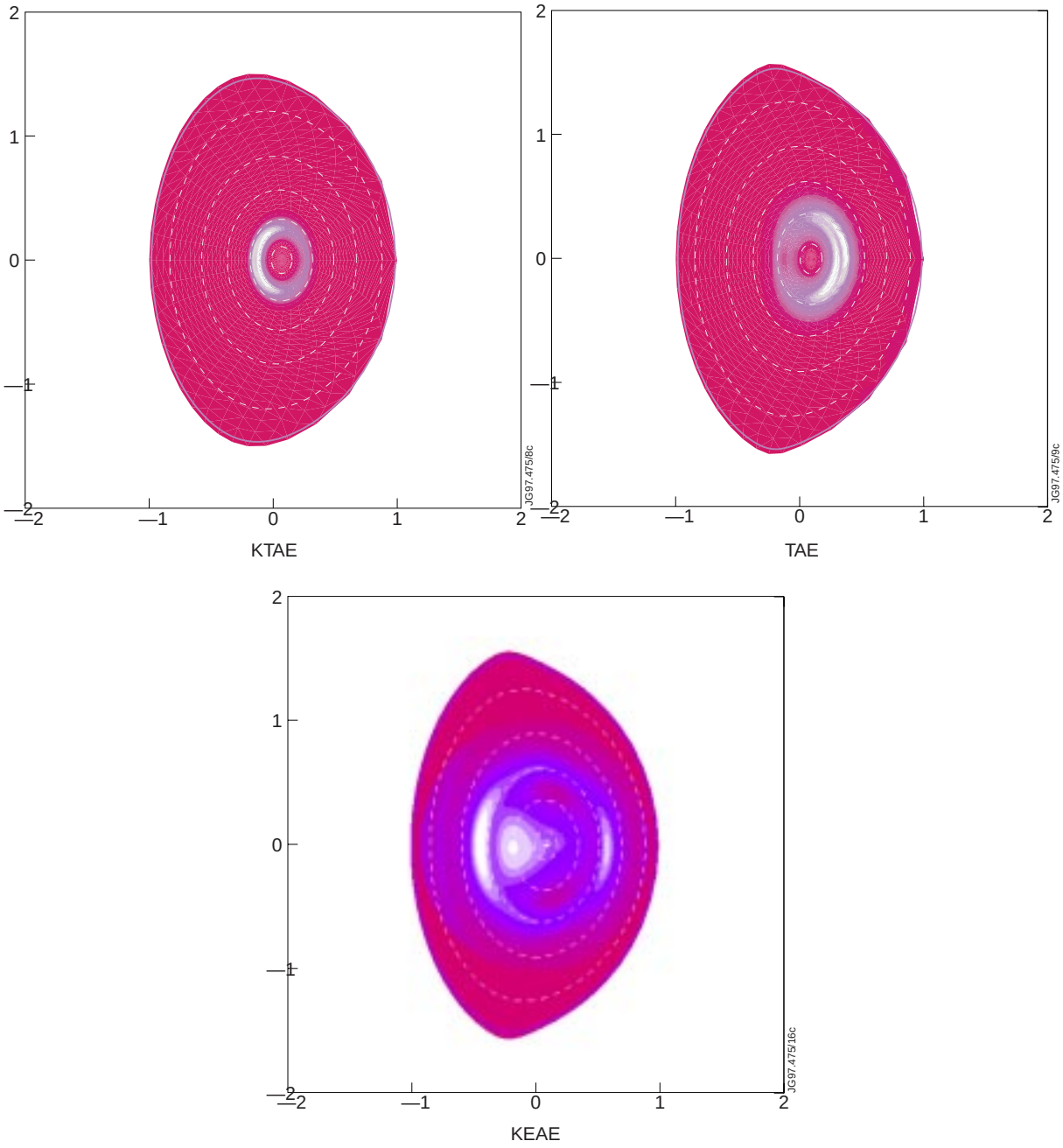

Fig. 2.8 Eigenfunctions of different types of AE's.

modes follow closely the Alfvén wave scaling in time. The mode numbers are n = ± 1, + 2 and ± 3. An analysis of the magnetic response in the range of the elliptic gap shows that initially there are several signals with negative mode numbers and few with positive n. With increasing time the modes with negative n disappear and more modes with positive n appear. Multiple modes are observed for each n. It is emphasised that this multiplicity is different from the fine-splitting of the TAE frequency as discussed above.

Since the drive is proportional to - $n\omega_*$ a negative n should correspond to a positive pressure gradient. The reconstruction of the heating deposition reveals that initially the energy density of the RF generated ions is hollow, i.e. $\frac{d}{dr}P_{fast}$ has positive sign in the core as displayed in

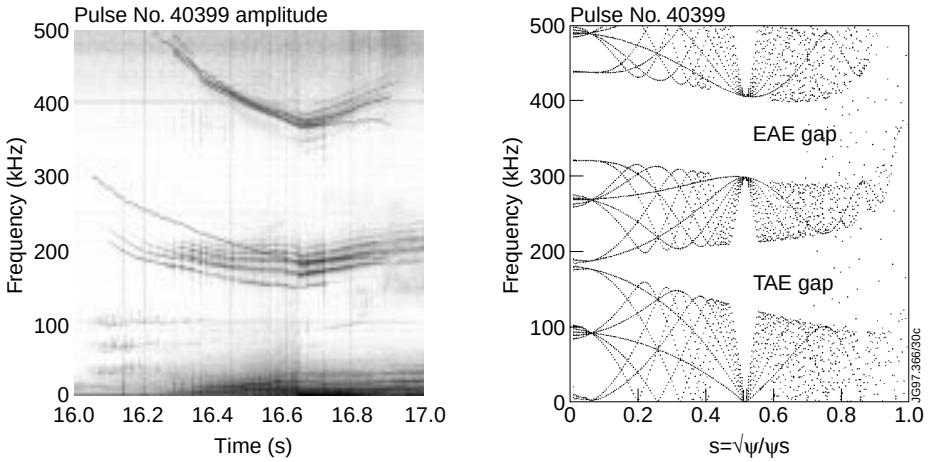

Fig. 2.9 AE activity in optimised shear discharge #40399 a) Spectrogram: frequency versus time (The solid line indicates the prognosticated Alfvén frequency for central gap value for safety factors). b) Continuous spectrum gap structure.

Fig. 2.10. With increasing time the magnetic axis shifts outwards to the resonance layer and the fast ion density profile has monotonic character. This is consistent with the experimental evidence that EAE's with negative wave number become less pronounced with increasing time. The eigenfunction of the EAE is characterised by coupling through toroidal and elliptic effects, i.e. a poloidal harmonic m couples at least with the m + 1 and m + 2 harmonics. Therefore, the coupling of the EAE with kinetic Alfvén waves in the gap region produces kinetic EAE's with both ballooning and anti-ballooning components. The global KTAE with p = 0 radial nodes in the elliptic gap region is plotted in Fig. 2.8. These KEAE's (with p = 0,1,2,3 .....) are characterised by regular spacing Δω. The damping is only weakly increasing with increasing radial mode number in the gap. Consequently, such a sequence of KEAEs is a good candidate for the observed multiplicity of AE's. Details of the spectrum in the elliptic gap, with frequencies between 350 kHz and 420 kHz for the time slice of 35 ms following 46.5 seconds in the discharge is shown in Fig. 2.11. The modes with negative mode numbers n = - 1, - 3 have quite small amplitudes. We therefore concentrate on the AE's with n = + 1, + 2. A multiplicity of four is observed for both n values. The spacing of the modes

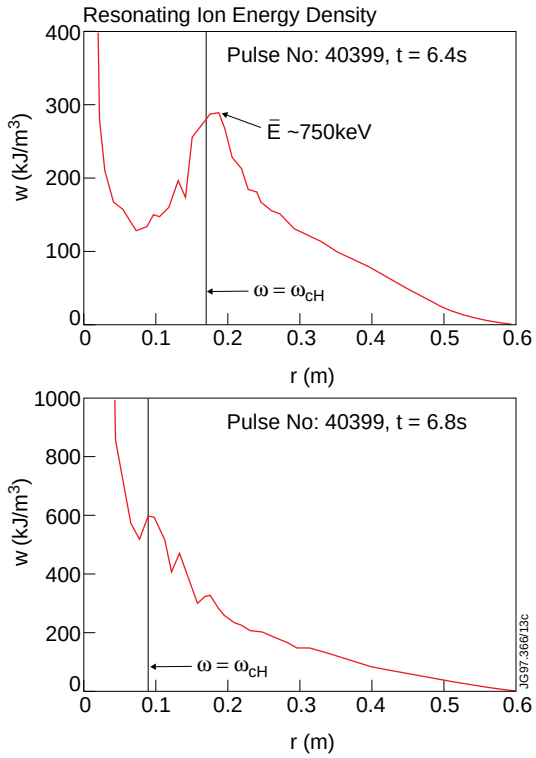

Fig. 2.10 Energy density profile of ICRH accelerated ions at different times. The magnetic axis moves towards the ion cyclotron resonance layer in time.

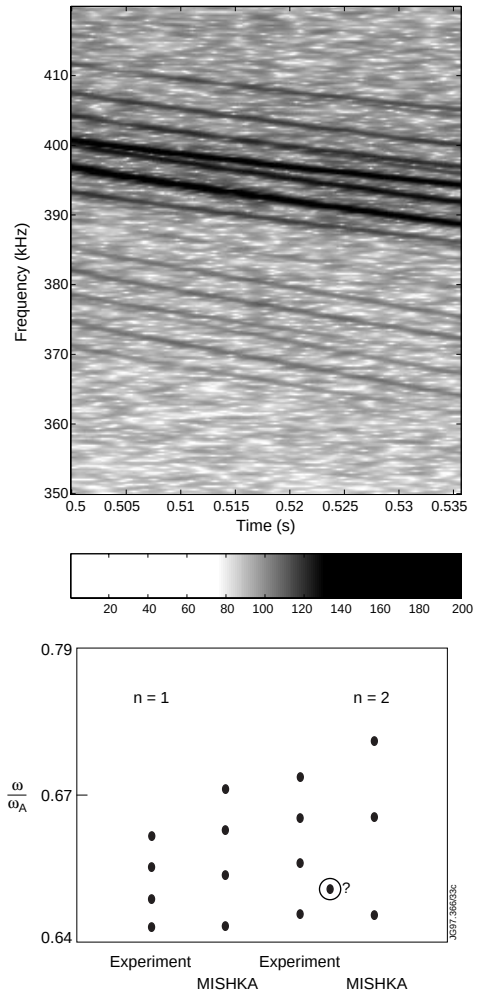

Fig. 2.11 a) Details of elliptic gap on spectrogram of Fig. 2.10a. b) Kinetic effects on EAE computed by the MISHKA code with complex resistivity Im (η) = - 1.16 × 10^{-6}; Re (η) = 4.8 × 10^{-8}.

relative to each other is almost constant. Inserting the discharge equilibrium profiles for density, safety factor and T_i and T_e profiles yields the value of the complex resistivity factor used in the MISHKA code of

$$\text{Im}\,(\eta) = -\,1.16 \times 10^{-6},\ \text{Re}\,(\eta) = 4.8 \times 10^{-8} \qquad (2.25)$$

The code produces indeed a sequence of Kinetic Eliptical Alfvén Eigenmodes with almost constant frequency spacing for n = + 1 and + 2 with slightly increasing radiative damping as displayed in Table II. Completely equal spacing in frequency and damping can occur only for a single gap. Due to a more complicated radial structure some deviation has to arise.

These eigenfrequencies ω lie within 5% of the measured frequency when the Doppler shift correction is performed. However, the frequency spacing Δω differs from the measured one by a factor of approximately 1.5 due to the uncertainty in the non-ideal parameter (2.7). It is noted that one observed mode with n = 2 does not have a clear structure; rather, it appears to be a mixture of n = 1 and n = 2. The corresponding frequency is marked by a question mark on Fig. 2.11. This indicates that the identification of the observed spectrum of AE's with

n	p	ω	$-\gamma_d$	n	p	ω	$-\gamma_d$
1	0	0.641	0.0001	2	0	0.646	0.00072
	1	0.653	0.00053		1	0.665	0.00094
	2	0.662	0.00046		2	0.681	0.00092
	3	0.671	0.00077		3	0.697	0.0014
	4	0.680	0.00078		4	0.725	0.0013

frequencies in the elliptic gap agrees within the accuracy of the plasma parameters with the computed KEAE's.

The destabilisation of AE's by alpha particles in D-T plasmas is currently under investigation in the JET DTE1 experiments. Two types of discharges have the potential of achieving high fusion power in excess of 10MW fusion power, namely the hot-ion H-mode and the optimised shear scenario characterised by an internal transport barrier. From relevant D-D plasmas the alpha-particle profiles are computed by the TRANSP code. The stability analyis has been performed by the CASTOR-K code. The corresponding results are presented in Fig. 12a). A typical Hot-ion H-mode is characterised by a value of q on axis around $q_0 \approx 0.8$. Consequently, the global AE which is first destabilised is a n = 5 KTAE due to its small radiative damping. The eigenfunction is localised in the plasma core. A slightly different q-profile or alpha particle pressure will interact preferably with similar modes, such as n = 6 KTAE. In Fig. 12a, the stability boundary is plotted in the plane of alpha particle beta and electron density (the ratio of the α-birth velocity to the Alfvén speed is $V_\alpha / V_A \propto \sqrt{n_e}$). It is evident that the first D-T discharge on JET, shot 26148 (see Ref. [21]) is found to be stable due to the small β_α in the case of $P_{fus} \approx 2$ MW. No activity has been observed in this discharge. The high performance D-D discharge #26087, treated now as a fictitious D-T discharge, has sufficiently high alpha pressure for instability. But, due to the significant ion Landau damping in this high density plasma, the unstable domain is not reached. For an n = 5 core localised KTAE in a D-T plasmas the alphas provide a drive of $\gamma/\omega_A = 1\%$, whereas the damping is 0.25% on thermal tritium, and 0.5% on thermal deuterium. The radiative damping is found to be 0.1%. Thus, the resulting instability has a growth rate of $\gamma/\omega_A = 0.15\%$. It is noted, however, that low-density discharges, such as the equivalent of D-D shot #38093, should produce an instability drive sufficient to overcome the damping. Thus, it is conjectured that on JET D-T plasmas alpha particles can drive specific KTAE unstable. The damping can be further reduced by switching-off the neutral beam heating whereas the drive is maintained during the slowing-down of the alphas for more than 0.5 seconds. This scenario has successfully been demonstrated on TFTR [22].

The stability boundaries for optimised shear plasmas are shown in Fig. 12b. These discharges are characterised by q profiles which well-exceed unity everywhere, i.e. $q_{min} \approx 1.5 - 2$, but not fully reversed. Due to the more peaked alpha pressure profile AE of low-n can be driven unstable and the AE of interest is a TAE/KTAE with n = 2. It is seen that for small plasma

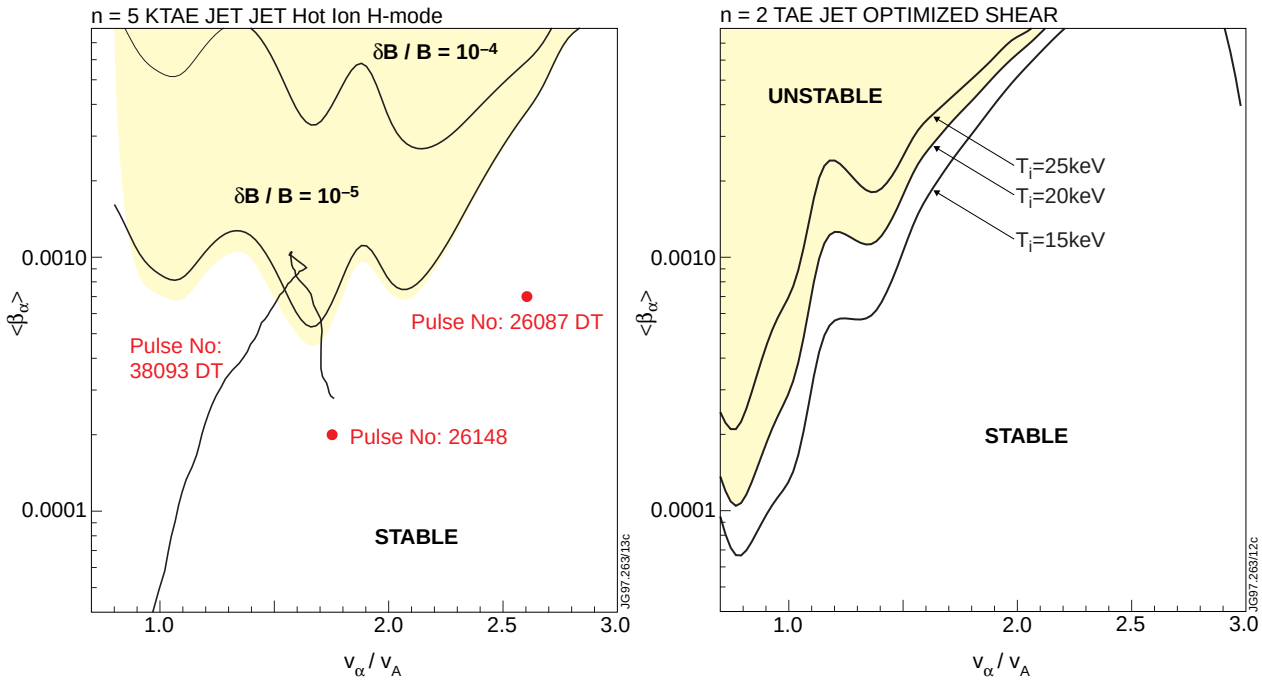

Fig. 2.12 Stability diagram of typical JET DTE1 discharges a) n = 5 KTAE in hot-ion H-mode. b) n = 2 TAE in optimised shear.

densities, instabilities occur for $\beta_\alpha \geq 0.02\%$ – a value significantly lower than in the hot-ion H-mode plasmas. Again it is found that α's can destabilise these TAE's. A heating power switch-off will reduce the damping significantly. These discharges have, in addition, RF heating in the range of $P_{RF} \approx$ 4-6 MW. Thus, AE's should definitely be observed for combined drive in this class of JET discharges.

3. WEAK TURBULENCE MODEL

It has been established that in the case of a weak drive only normal modes of the bulk plasma can be excited by resonant interaction with energetic ions. In terms of the normalisation used in CASTOR-K, the growth rate γ/ω_A (with ω_A the Alfvén frequency on axis) and the damping rate γ_d/ω_A typically have magnitudes on the order of a few times 10^{-3} . The dominant damping mechanisms are normally radiative (continuum) and ion Landau damping. In the context of alpha particle-wave interaction, the drive provided by the pressure gradient, $d\beta_{fast} / dr$, must overcome the indicated background damping for instability. It has been further established experimentally on JET that AE with such small damping persist in JET plasmas. This indicates that the perturbative approach is suitable for the description of the nonlinear evolution of the fast ion distribution and wave amplitude. Therefore, in this modelling, the radial wave structure will be maintained, but the amplitude and the phase of the wave will change:

$$\xi\,(\mathbf{r},t) \rightarrow A\,(t)\,\xi\,(\mathbf{r})\,e^{iC(t)} \qquad (3.1)$$

3.1 Wave Evolution

A Lagrangian formalism for wave particle interaction has been applied to the time evolution of the Alfvén waves [23]. Starting from the Lagrangian for charged particles in an electromagnetic field

$$L = \sum_{\text{particles}} \left(\frac{mv^2}{2} + \frac{e}{c}(\mathbf{Av}) - e\phi_e \right) \tag{3.2}$$

$$+ \frac{1}{8\pi} \int \left(\mathbf{E}^2 - B^2 \right) dV \ ,$$

where **A** and ϕ_e denote the vector and scalar potentials and E the electric field, the Lagrangian can be decomposed when the growth develops on a time scale asymptotically longer than the equilibrium

$$L = L^{(o)}(\omega_o) + L^{(1)} \ . \tag{3.3}$$

Variation of $L^{(o)}$ yields the fluid waves, whereas variation of $L^{(1)}$ gives the time evolution of the mode. This decomposition of the times scales coincides with the application of the perturbative method already applied in the evolution of the power transfer between energetic particles and waves

$$\frac{\partial}{\partial t} \sim \gamma << \omega_o \quad \text{and} \quad \Delta\omega << \omega_0 \ . \tag{3.4}$$

Here, ω_o represents the frequency of an AE and $\Delta\omega$ is the change in frequency. However, by incorporating the results of the linear phase a wave Lagrangian can be derived for the combined response of the background plasma and the electromagnetic field which only depends on the amplitudes and phases of the linear waves as introduced in equation (3.1). Following Ref. [23] $L^{(1)}$ can be expressed as a sum over the number of waves n_w;

$$L_w^{(1)} = \sum_k \frac{E_k}{\omega_k} \left[A_k^2 \, \dot{C}_k \right] \tag{3.5}$$

with E_k denoting the energy of the Alfvén wave per unit amplitude.

It is noted that in the case of a strong drive non-normal modes of the system can be driven unstable, by overcoming the underlying continuum damping. This gives rise to the so-called Energetic Particle Mode (EPM), which has been studied extensively in the literature [24]. Experimental evidence of such EPM's has been obtained for fishbones [25]. In JET plasmas,

however, the power density seems to be below the threshold to drive EPMs. Furthermore, the isotropic α-particle generation in JET DTE1 and in ITER plasma is spread over half the plasma radius. These considerations indicate that the perturbative approach is suitable for JET and ITER plasmas. We describe now in detail the algorithm for the nonlinear interaction of fast ions with Alfvén waves in toroidal plasmas.

The complex phase factor in the wave Eq. (3.1) is decomposed into real and imaginary parts

$$X_k = \mathrm{Re}\left\{A_k e^{iC_k}\right\} = A_k \cos C_k \tag{3.6a}$$

$$Y_k = \mathrm{Im}\left\{A_k e^{iC_k}\right\} = A_k \sin C_k \tag{3.6b}$$

It has proven useful to introduce more generalised coordinates ψ, θ, ξ where the generalised toroidal angle is defined as $\xi = \phi - \nu(\theta, s)$, together with a choice of the Jacobian such that JB^2 is a flux function (see Ref. [26]).

Further the perturbed field is expressed in the following restricted form being valid for Alfvén waves in low beta plasmas

$$\delta\mathbf{B} = \nabla \times (\xi \times \mathbf{B}) \rightarrow \nabla \times (\mathbf{b}\ \delta A_{\|}) = \nabla \times (\alpha\mathbf{B}) \tag{3.7}$$

where the function $\alpha(\mathbf{r})$ is constructed from the MHD normal mode $\delta\mathbf{B}$. Eventually the perturbed potential as seen by a specific particle (index j) is given by a sum of n_w waves

$$\alpha_j = \frac{1}{B_j} \sum_{k=1}^{n_w} \sum_{m=m_k^-}^{m_k^+} \frac{k_{\|m}}{\omega_k} \left[X_k(t) \cos\theta_{jkm} + Y_k(t) \sin\theta_{jkm} \right] \phi_{km}\left(\psi_j\right) \tag{3.8}$$

where

$$\theta_{jkm} = n_k\, \xi_j - m_k\, \theta_j - \omega_k t \tag{3.9}$$

$$k_{\|m} = (nq - m)/JB \tag{3.10}$$

The summation over m refers to the Fourier decomposition and $\phi_{km}(\psi_j)$ to the corresponding radial eigenfunction as computed by the MHD codes MISHKA-1 and CASTOR. Variation of the perturbed Lagrangian then yields the equations.

$$\frac{d}{dt} X_k = \frac{1}{2E_k} \sum_{j=1}^{n_p} \delta n_j \sum_{m=m_k^-}^{m_k^+} \left(\omega_k - k_{\|m} v_{\|j}\right) \sin\theta_{jkm}\ \phi_{km}\left(\psi_j\right) - \gamma_d\ X_k \tag{3.11a}$$

$$\frac{d}{dt} Y_k = \frac{1}{2E_k} \sum_{j=1}^{n_p} \delta n_j \sum_{m=m_k^-}^{m_k^+} \left(\omega_k - k_{\|} v_{\|j}\right) \cos\theta_{jkm}\ \phi_{km}\left(\psi_j\right) - \gamma_d\ Y_k \tag{3.11b}$$

where we have added a linear background wave damping γ_d. The energy of the kth wave is given by

$$E_k = \frac{1}{2}\int \frac{dv}{v_A^2} \left|\nabla_\perp \phi_k\right|^2 . \tag{3.12}$$

3.2 δf method

The fast ion distribution is represented in the form

$$f = F_o\,(\varepsilon, P_{0\phi}, \mu) + \delta f_a\,(\underline{r}, \underline{v}, t) + \delta f_{na}\,(\underline{r}, \underline{v}, t) \tag{3.13}$$

where F_o is the equilibrium distribution, δf_a the fluid-like contribution to the fast-ion response and δf_{na} the non-adiabatic response. Only the non-adiabatic response needs to be evaluated to obtain the particle-to-wave power transfer. The time evolution equation reads

$$\frac{d}{dt}(\delta f_{na})_j = -\dot{P}_\phi \left.\frac{\partial F_0}{\partial P_{0\phi}}\right|_j - \dot{H}\left.\frac{\partial F_0}{\partial \varepsilon}\right|_j \tag{3.14}$$

The fact that only the deviation from the initial distribution is evaluated leads, in particular in the linear phase, to substantial noise reduction and gain in numerical accuracy as well as in CPU time.

3.3 Fast Particle motion

A Guiding Centre Hamiltonian method (see Ref. [26]) is applied for following the particle motion. Based on the coordinate system and choice of representation introduced in Sec. 3.1, the Hamilton's equations are

$$\dot{P}_{\zeta j} = v_{\|j} B_j \frac{\partial \alpha_j}{\partial \zeta}\frac{\partial \Phi_j}{\partial \zeta_j} \tag{3.15a}$$

$$\dot{P}_{\theta j} = v_{\|j} B_j \frac{\partial \alpha_j}{\partial \theta_j} - \frac{\partial \Phi_j}{\partial \theta_j} - \left(v_{\|\,j}^2 + \mu_j B_j\right)\frac{1}{B_j}\frac{\partial B_j}{\partial \theta_j} \tag{3.15b}$$

$$\dot{\zeta}_j = \frac{v_{\|j} B_j}{D_j}\left(q_j + \rho_j \frac{\partial I_j}{\partial \psi_j}\right) + \frac{I_j}{D_j}\Lambda_j \tag{3.15c}$$

$$\dot{\theta}_j = \frac{v_{\|j} B_j}{D_j}\left(1 - \rho_j \frac{\partial g_j}{\partial \psi_j}\right) - \frac{g_j}{D_j}\Lambda_j \tag{3.15d}$$

with

$$\Lambda_j \equiv \nu_{\|j} B_j \frac{\partial \alpha_j}{\partial \psi_j} - \frac{\partial \Phi_j}{\partial \psi_j} - \left(\nu_{\|}^2{}_j + \mu_j B_j \right) \frac{1}{B_j} \frac{\partial B_j}{\partial \psi_j} \tag{3.16a}$$

$$D_j \equiv \rho_j \left(g_j \frac{\partial I_j}{\partial \psi_j} - I_j \frac{\partial g_j}{\partial \psi_j} \right) + I_j + q_j g_j \tag{3.16b}$$

In practice, it is more convenient to integrate ψ_j forward in time and then evaluate $P_{\theta j}$ explicitly using Eq. (3.13b) rather than evolve $P_{\theta j}$ forward and attempt to invert Eq. (3.13a) for ψ_j. In terms of differential quantities, the equation for $\dot{\psi}_j$ is

$$\dot{\psi}_j = \frac{g_j}{D_j} \dot{P}_{\theta j} - \frac{I_j}{D_j} \dot{P}_{\psi j} \tag{3.17}$$

The nonlinear numerical model is a $(5 \times n_p + 2 \times n_w)$ - dimensional system of ordinary differential equations for the particle variables $P_{\psi j}$, ψ_j, ϕ_j, θ_j, δf_j together with the wave amplitudes X_k, Y_k. This algorithm has been given the name FAC, for Fast particle Alfvén wave interaction Code [27].

A similar numerical algorithm is employed in the HAGIS code [28]. In comparison with the FAC code it allows treatment of more general equilibria, in particular JET discharges; but at the expense of significantly larger CPU time requests. The three codes CASTOR-K, FAC and HAGIS have been developed over an extensive period simultaneously at JET and Culham setting off many cross-checks of the algorithms and numerical schemes. The results shown in Fig. 2.4 demonstrate the good agreement of the different methods in the linear regime.

The simplest illustration of the nonlinear saturation of the mode comes from the solution of the initial value problem, without any background damping of the wave and without particle sources. The mode then grows until all the particle free energy is transformed into the wave energy and the distribution function flattens near the resonance. The corresponding saturation level is determined by the condition $\omega_b = \gamma$, where ω_b is the nonlinear bounce-frequency of the resonant particle in the wave, and γ is the linear instability growth rate. The bounce frequency is proportional to the square root of the amplitude, which leads to the analytic estimate

$$\frac{\delta B}{B} = c_b \left(\frac{\gamma}{\omega} \right)^2 . \tag{3.18}$$

This scaling constitutes a good test for the nonlinear code. In particular for parameters which are of relevance for a high performance JET hot-ion discharge, which could produce fusion power in excess of 10 MW in the JET DTE1 campaign, KTAE with toroidal mode numbers of n = 5 to n = 8 are found to be most unstable as discussed in Sec. 2.4. Such KTAE's should

be preferably destabilised. By varying the alpha particle pressure in the simulation the initial linear growth rate γ/ω_A is varied. The result concerning the saturation amplitude for both independent and interacting KTAE's is displayed in Fig. 3.1. The result clearly shows a quadratic dependence of $\delta B/B$ on γ/ω_A with the proportionality factor $c_b \approx 1$. This dependence has also been confirmed for ITER simulations, where a set of high-n KTAE's is considered, as displayed in Fig. 3.1.

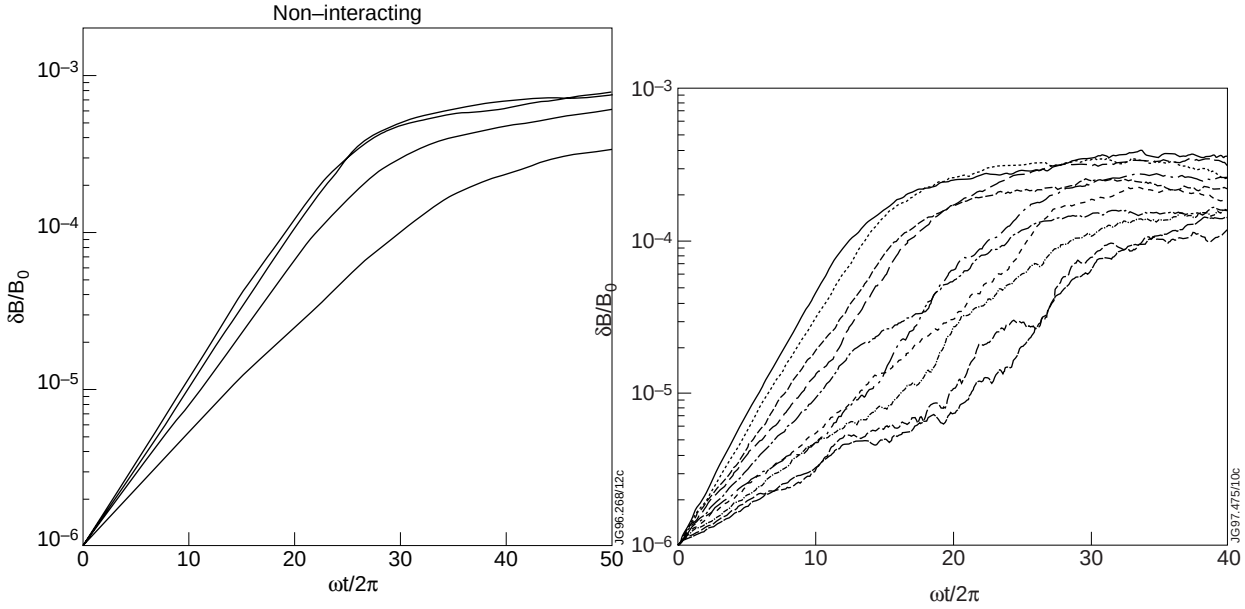

Fig. 3.1 Nonlinear evolution of AE amplitudes computed by the FAC code in the absence of sources and damping. a) for n = 5 to 8 KTAE at JET. b) for high-n AE's at ITER. The saturated amplitude scales as $\frac{\delta B}{B} \propto C_b\left(\frac{\gamma}{\omega}\right)^2$ with $C_b \simeq 0.5$

The second important result for these specific cases neglecting sources and damping is that the onset of orbit stochasticity sets a threshold in the perturbed field of about 10^{-3},

stochasticity threshold: $$\left(\frac{\delta B}{B}\right)_{cr} > (0.5-1)\times 10^{-3}\,. \qquad (3.19)$$

Such levels in the perturbed field are not expected to be reached by the α-particle drive in DTE1 tritium plasmas.

We can analyse the particle redistribution in more detail. An effective reduction of the instability drive is achieved by pushing the fast resonating ions out of resonance by a radial displacement. In the case of a barely passing particle the orbit can be changed into a trapped orbit. For a large banana width near the plasma edge the particle is lost by one such impact. Such losses are called prompt losses, and the TAE induced prompt losses are similar to ripple induced losses. In both cases the loss rate is proportional to the magnetic field perturbation. In tokamaks, which are designed for good alpha-particle confinement and are characterised by a very small

gyro-radius relative to the minor radius and a small ripple, the fast particles are displaced mostly radially but remain in the plasma. This is indicated in Fig. 3.2. Resonance overlap is required to obtain TAE induced diffuse losses. The loss rate scales quadratically with the perturbed field.

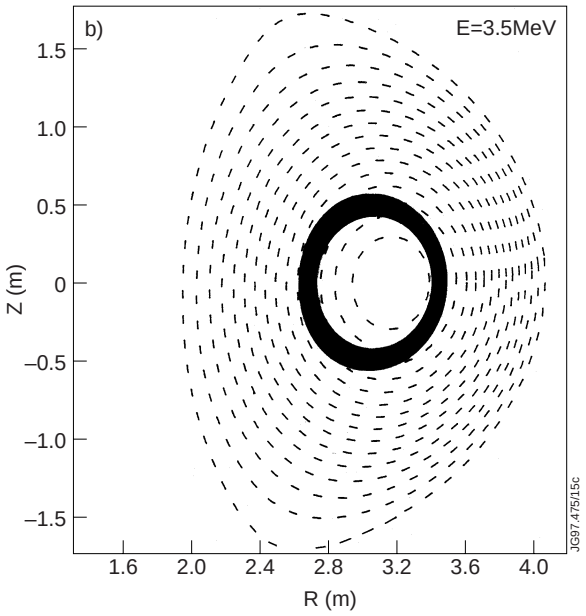

Fig. 3.2 Stochastic radial diffusion caused by a single AE computed by HAGIS.

In TFTR the losses due to NBI driven TAE and AFM (Alfvén Frequency Modes) have been examined by Darrow et al [29]. The losses in the plasma centre are measured by neutron emission and the fast ion losses to the wall during bursts of AE activity by detectors. It was found that the change in the neutron rate scales linearly with the perturbed amplitude during bursts, i.e. like prompt losses. The losses detected outside the plasma scale quadratically with the amplitude during bursts, i.e. like diffusive losses.

If weak background damping is present (with the damping rate $\gamma_d << \gamma_L$), the saturated state can only last on the time scale shorter than the damping time, $1/\gamma_d$, i.e. the wave energy damps after saturation, whereas the distribution function remains flat at the resonance. The overall evolution of the amplitude in this case looks like an isolated burst (wave build-up from the instability and wave damping after the distribution flattens).

If there is a relaxation mechanism that restores the resonant particle distribution after the burst, subsequent bursts will appear, resulting in a continuous pulsation scenario. The time interval between the pulses is determined by the distribution function reconstitution time near the resonance. An example of these nonlinear bursts is shown in Fig. 3.3.

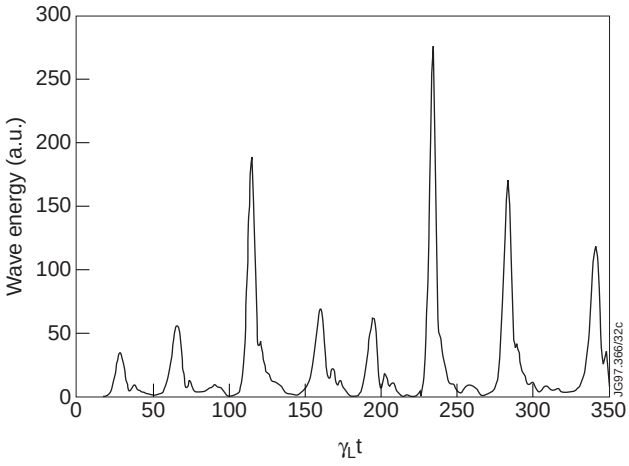

Fig. 3.3 Pulsating non-linear regime for an isolated TAE mode. The normalised background damping and particle relaxation rate for this run are, respectively, γ_d/γ_L = 0.15 and ν_a/γ_L = 0.03.

If the particle source is strong enough to reconstitute the distribution near the resonance within the wave damping time, the bursts merge together and a driven steady state establishes. In this saturated state, the background dissipation is balanced by the constant power supplied by the particle source. The steady state distribution function near the resonance results from

a balance between flattening by the wave and reconstitution from the source. The corresponding saturation level of the mode has been found in Ref. [31] and it is given by

$$\omega_b^2 \cong \nu_{eff}^2 \left(\frac{\gamma_L}{\gamma_d} \right)^{2/3} \left(1 - \frac{\gamma_d}{\gamma_L} \right)^{1/2} \tag{3.20}$$

where ν_{eff} denotes the effective pitch angle scattering frequency.

In most experiments the energetic particle pressure that determines γ_L builds up slowly compared to the characteristic growth time of the instability. Therefore the system typically spends a long time near the instability threshold, where γ_L equals or slightly overcomes the damping rate. The near-threshold regimes have been studied in Ref. [30]. although these near-threshold regimes allow both the steady-state and the pulsation scenarios, the scaling laws for the saturation level and pulsations are now governed by the small parameter

$$\varepsilon = (\gamma_L - \gamma_d) / \gamma_d << 1 \tag{3.21}$$

The transition from the steady state to pulsations is determined by the ratio of the collisional relaxation rate of resonant particles, ν_{eff}, to the linear instability growth rate, $\gamma = \gamma_L - \gamma_d$. Note that ν_{eff} is typically much greater than the particle 90° pitch-angle scattering rate ν (either classical or anomalous); ν_{eff} scales roughly as $(\nu\omega^2)^{1/3}$, where ω is the mode eigenfrequency [32]. The system always evolves to the steady state when $\nu_{eff} >> \gamma$. As γ increases to the values comparable to the ν_{eff}, this steady state becomes unstable. A bifurcation occurs at γ of the order of ν_{eff}, giving rise to a periodic limit cycle behaviour. At even larger values of gamma additional bifurcations occur, which break the periodicity of the first cycle, and eventually lead to an explosive evolution of the mode [30]. It is plausible that the transition from the steady state saturation to the limit cycle can explain the “pitchfork” in the TAE spectrum shown in Figs. 3.4. This pitchfork-type splitting in the TAE spectrum occurs, when the RF heating power well exceeds the threshold for TAE excitation, as discussed in detail on Fig. 2.5 in Sec. 2.4. We conjecture that the modes first exhibit a steady state near-threshold saturation, that evolves slowly due to RF heating. At the point when the growth rate reaches the stability limit for this nonlinear steady state, the mode bifurcates and develops a limit cycle. The moment of bifurcation for each spectral line on Fig. 3.4 can be identified as the moment of line splitting.

Another interesting phenomenon observed in JET and other tokamaks [33-35], which is likely to have a nonlinear nature, are the modes with time-dependent frequencies (“chirping” modes) see Fig. 3.5. In Fig. 3.5, RF driven chirping modes on JET are shown. Unlike the TAE modes, whose frequency cannot change fast since it is determined by the equilibrium plasma parameters (the gap location, plasma density etc.), these modes exhibit very fast chirping at the time scale of ~10 msec. These modes don’t seem to be background plasma eigenmodes. It is more likely that they are Bernstein-Greene-Kruskal type nonlinear waves, whose existence

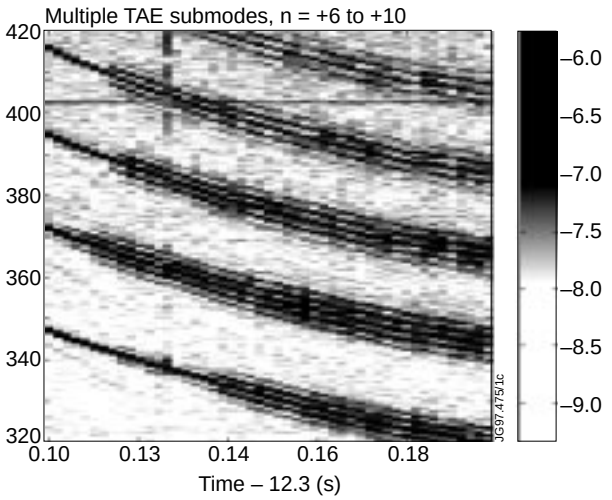

Fig. 3.4 Detail of spectrogram of RF driven AE's showing "pitch fork"-type fine splitting of TAE frequency.

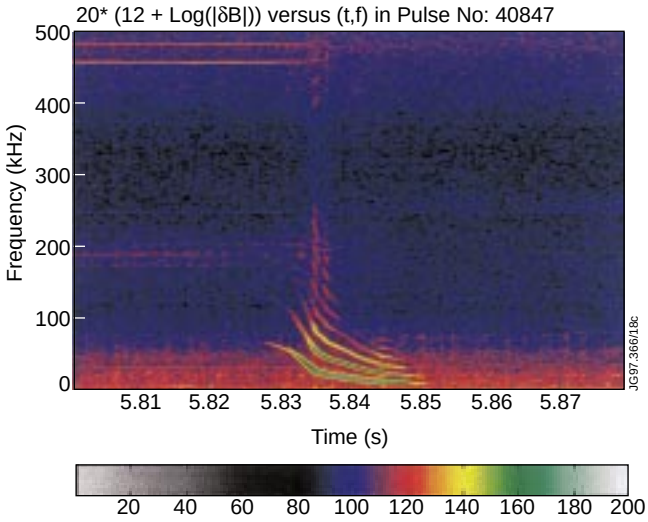

Fig. 3.5 RF driven "chirping" modes.

requires strong local perturbations of the phase-space distribution of energetic particles. These modes may result from the nonlinear evolution of the linearly unstable Energetic Particle Modes (EPM) [24], although this may not be the only mechanism. The EPMs are non-perturbative kinetic modes that generally exhibit fast chirping in the nonlinear regime [24, 37]. Also the BGK-type modes can chirp when there is a background dissipation in the system [36]. A more detailed analysis is needed to check whether the experimentally observed chirping can indeed be explained by one of the mechanisms mentioned above.

Both the experimental data and the theoretical analysis indicate that isolated modes are not likely to cause any macroscopic re-distribution of energetic particles under reactor conditions. Such a redistribution generally requires multiple modes with overlapping resonances in accordance with the Chirikov criterion [38]. In some cases the resonance overlap can lead to an avalanche type response when the overlap of a few neighbouring resonance triggers an overlap in a broad area of phase space (so-called domino effect). Single mode studies allow us to quantify the condition of resonances overlap for different saturation regimes. Once the resonance overlap is achieved, the particles experience macroscopic stochastic diffusion like in the case shown in Fig. 3.2. The stochastic area in Fig. 3.2 is limited to a band where the "active" resonances are localised. If these resonances extend all the way to the edge of the plasma, particle loss can occur. Otherwise the particles will be redistributed internally, which may even be beneficial.

4. CONCLUSIONS

During recent years the physics of Alfvén Eigenmodes has been established as a fundamental branch of magnetic fusion physics. Both experimental and theoretical tools have advanced to the state where detailed discharge analysis is now feasible and is being performed routinely on the

major tokamak experiments. The interfacing of measured spectra with computed AE spectra is applied to the verification of the accuracy of measured plasma profiles.

In this paper a linear model for the evaluation of the power transfer between energetic ions and waves is described in conjunction with details of the numerical solution applied in the CASTOR-K code. Citation to methods from other groups is included. The application of the CASTOR-K code to specific antenna, RF, and α-particle driven excitation of AE is discussed ("spectroscopy"). The Alfvén-type scaling of the experimentally observed spectra has been verified. The threshold in RF power for TAE excitation in the range of 5MW is consistent with modelling. Kinetic effects give rise to a weakly damped spectrum of kinetic EAE's. In addition, scenarios for the existence of alpha particle driven AE in JET D-T discharges, in particular, for low-density plasmas, are discussed. The perturbative approach, where the radial eigenmode structure is established by linear theory, but variation of amplitude and phase introduced, can be extended into a self-consistent weak turbulence model. The codes FAC and HAGIS being used at JET, as well as corresponding codes at other laboratories, allow a quantitative analysis of the fast ion loss/redistribution due to collective effects. A comprehensive discussion of the different types of nonlinear solutions is presented, i.e. the conditions for steady-state saturation, bursts and chirping modes are outlined. The applications of the JET codes to the problem of mode saturation are discussed. Therefore the nonlinear wave evolution and particle redistribution can be very complex, in particular for ignited plasmas.

In JET DTE1, it is expected that alpha particle driven AE's should be observed when the damping is kept small, such as by low-density or by switching-off the neutral beams.

REFERENCES

[1] Rosenbluth, M.N., and Rutherford, P.H., Phys. Rev. Lett. **34**, 1428 (1975).

[2] Mikhailovskii, A.B., Sov. Phys. JETP **41**, 890 (1975).

[3] Duong, H.H., et al., Nuclear Fusion **33**, 749 (1993).

[4] Fasoli, A., et al., Phys. Rev. Lett. **75**, 645 (1995).

[5] Fasoli, A., et al., Phys. Rev. Lett. **76**, 1067 (1996).

[6] Fasoli, A., et al., Nuclear Fusion **35**, 1485 (1995).

[7] Mikhailovskii, A.B., Huysmans, G.T.A., Kerner, W.O.K., and Sharapov, S.E., Plasma Phys. Rep., **23**, 844 (1997).

[8] Kerner, W., et al., JET-P(97) 04 to appear in Journ. Comp. Phys.

[9] Mett, R.R., and Mahajan, S.M., Phys. Fluids **B4**, 2885 (1992).

[10] Berk, H.L., Mett, R.R., and Linberg, D.M., Phys. Fluids **B5**, 3969 (1993).

[11] Candy, J., and Rosenbluth, M.N., Phys. Plasmas **1**, 356 (1994).

[12] Breizman, B.N., and Sharapov, S.E., Plasma Phys. Contr. Fusion **37**, 1057 (1995).

[13] Connor, J.W., et al., Proceed. XXI EPS Conference on Contr. Fusion Plasma Phys. **18B**, Part III, 616 (1994).

[14] Poedts, S., Schwarz, E., Journ. Comp. Phys. **105**, 165 (1993).
[15] Porcelli, F., Berk, H.L., Stankiewicz, R., and Kerner, W., Phys. Plasmas **1**, 470 (1994).
[16] Borba, D., Candy, J., Kerner, W., Sharapov, S., JET-P(96)35.
[17] Abramowitz, M., and Stegun, I.A., Handbook of Math. Functions, Dover Publications, New York (1970).
[18] Eriksson, L.-G., Hellsten, T., and Willén, V., Nucl. Fusion **33** (1993) 1037.
[19] Carlsson, J., Hellsten, T., and Eriksson, L.-G., Fido, a code for computing the resonant-ion distribution function during ICRH. Royal Institute of Technology Report ALF-1996-104, Stockholm (1996).
[20] Fasoli, A., et al., invited paper at 24th EPS to be published in Plasma Phys. Control. Fusion.
[21] The JET Team, Nucl. Fusion **32**, 197 (1992).
[22] Nazikian, R., et al., Alpha Particle Driven Toroidal Alfvén Eigenmodes in TFTR, JAERI-memo 09-124 (1997).
[23] Berk, H.L., Breizman, B.N., and Pekker, M.S., Nuclear Fusion **35**, 1713 (1995).
[24] Chen, L., Phys. Plasmas **1**, 1519 (1994).
[25] Mc.Guire, et al., Phys. Rev. Lett. **50**, 891 (1983)
[26] White, R.B. and Chance, M.S., Phys. Fluids **27**, 455 (1984).
[27] Candy, J., Borba, D., Berk, H.L., Huysmans, G.T.A., and Kerner, W., Phys. Plasmas **4**, 2597 (1997).
[28] Pinches, S.P., et al., to appear in Comput. Phys. Commun..
[29] Darrow, D.S., et al., Nucl. Fusion **7**, 939 (1997).
[30] Berk, H.L., Breizman, B.N., and Pekker, M.S., Phys. Rev. Letters **76**, 1256 (1996).
[31] Berk, H.L., Breizman, B.N., Phys. Fluids **B2**, 2226, 2235, 2246 (1990).
[32] Wong, K.L., et al., Phys. Plasmas **4**, 393 (1997).
[33] Heidbrink, W.W., Plasmas Phys. Contr. Fusion **37,** 937 (1995).
[34] Kusama, Y., et al., Confinement of ICRH-driven energetic protons and TAE-modes in JT-60U negative shear plasmas, JAERI-memo 09-124 (1997).
[35] Gryaznevich, et al., M.P., Proceed. 5-th IAEA Meeting on Alpha-particles in Fusion Research, 8-11 September 1997 (to be published).
[36] Berk, H.L., Breizman, B.N., and Petviashvili, N.V., Phys. Lett. A (to be published).
[37] Breizman, B.N., Berk, H.L., Pekker, M.S., Porcelli, F., Stupakov, G.V., Wong, K.L., Phys. Plasmas **4**, 1559 (1997).
[38] Chirikov, Phys. Reports **52**, 263 (1979).

.